THE JOURNAL OF BIOLOGICAL CHEMISTRY VOL. 281, NO. 20, pp. 14503–14513, May 19, 2006

The Electron Transfer Complex between Cytochrome c_{552} and the Cu_A Domain of the *Thermus thermophilus* ba_3 Oxidase

A COMBINED NMR AND COMPUTATIONAL APPROACH[*] [S] [◆]

Received for publication, February 6, 2006, and in revised form, March 16, 2006 Published, JBC Papers in Press, March 22, 2006, DOI 10.1074/jbc.M601108200

Lucia Muresanu[‡], Primož Pristovšek[§1], Frank Löhr[‡], Oliver Maneg[¶2], Marco D. Mukrasch[‡3], Heinz Rüterjans[‡], Bernd Ludwig[¶], and Christian Lücke[‡4]

From the [‡]Institute of Biophysical Chemistry, Center for Biomolecular Magnetic Resonance, J. W. Goethe-University, Marie-Curie-Strasse 9, D-60439 Frankfurt am Main, Germany, the [§]National Institute of Chemistry, Hajdrihova 19, SI-1000 Ljubljana, Slovenia, and [¶]Molecular Genetics, Institute of Biochemistry, J. W. Goethe-University, Marie-Curie-Strasse 9, D-60439 Frankfurt am Main, Germany

The structural analysis of the redox complex between the soluble cytochrome c_{552} and the membrane-integral cytochrome ba_3 oxidase of *Thermus thermophilus* is complicated by the transient nature of this protein-protein interaction. Using NMR-based chemical shift perturbation mapping, however, we identified the contact regions between cytochrome c_{552} and the Cu_A domain, the fully functional water-soluble fragment of subunit II of the ba_3 oxidase. First we determined the complete backbone resonance assignments of both proteins for each redox state. Subsequently, two-dimensional [^{15}N,^{1}H]TROSY spectra recorded for each redox partner both in free and complexed state indicated those surface residues affected by complex formation between the two proteins. This chemical shift analysis performed for both redox states provided a topological description of the contact surface on each partner molecule. Remarkably, very pronounced indirect effects, which were observed on the back side of the heme cleft only in the reduced state, suggested that alterations of the electron distribution in the porphyrin ring due to formation of the protein-protein complex are apparently sensed even beyond the heme propionate groups. The contact residues of each redox partner, as derived from the chemical shift perturbation mapping, were employed for a protein-protein docking calculation that provided a structure ensemble of 10 closely related conformers representing the complex between cytochrome c_{552} and the Cu_A domain. Based on these structures, the electron transfer pathway from the heme of cytochrome c_{552} to the Cu_A center of the ba_3 oxidase has been predicted.

Thermus thermophilus, a Gram-negative eubacterium originally isolated from hot springs, produces highly thermostable proteins under obligately aerobic conditions (1, 2). Its respiratory chain contains several major redox complexes, such as an NADH-oxidizing complex I (3) and a recently identified bc_1 complex (4). For this terminal part of the electron transport chain, *T. thermophilus* possesses two alternative pathways for oxygen reduction to water, depending on the oxygen partial pressure: (i) the cytochrome ba_3 oxidase branch with cytochrome c_{552} as water-soluble electron donor or (ii) the c_1aa_3 oxidase, where the *c*-type cytochrome domain is covalently bound to subunit II of this terminal oxidase (5).

Under low aeration conditions, the preferred product in *T. thermophilus* is the ba_3 branch (6, 7). Electron transport from the bc_1 complex to the ba_3 oxidase is mediated by the 14.4-kDa periplasmic cytochrome c_{552} (8). This *c*-type cytochrome contains a covalently bound heme moiety, with thioether linkages to two cysteine residues in a conserved Cys^{11}-Xaa^{12}-Yaa^{13}-Cys^{14}-His^{15} motif. The heme iron is octahedrally coordinated by the four porphyrin nitrogens and two axial ligands, His^{15} and Met^{69}, thus representing a "low spin" heme complex (9, 10). In the redox cycle, the iron atom alternates between the reduced, diamagnetic Fe^{2+} and the oxidized, paramagnetic Fe^{3+} state. Thereby, the reduced cytochrome c_{552} transfers one electron to the oxidized Cu_A domain, the first electron acceptor of the terminal ba_3 oxidase. From this solvent-exposed part of subunit II (11), the electron subsequently reaches the redox centers in the membrane-embedded subunit I, *i.e.* heme *b* and the binuclear heme a_3/Cu_B center where oxygen reduction takes place.

The entire ba_3 oxidase of *T. thermophilus* consists of subunits I, II, and IIa (874 residues, 84.9 kDa) and represents one of the smallest known terminal oxidases in both prokaryotic and eukaryotic organisms (12, 13). Moreover, contrary to most other members of the oxidase superfamily, this oxidase lacks most of the canonical amino acid "signatures" and was reported to pump only 0.5 H^+/e^- (13, 14). In the present NMR study, we use the Cu_A domain, the fully functional water-soluble fragment of subunit II. Its binuclear Cu_A center is asymmetric, with one copper atom (CU2) coordinated by His^{114}, Cys^{149}, Cys^{153}, and Met^{160} and the other (CU1) by the same two cysteine residues, His^{157} and presumably Gln^{151} (11, 13, 15). The charge of each copper atom alternates in the redox cycle between +1.5 ("mixed valence") and +1 (16, 17).

It had been shown previously (18, 19), that the complex formation between cytochrome c_{552} and the aa_3 oxidase of *Paracoccus denitrificans* is based on electrostatic interactions between the hydrophilic residues surrounding Trp^{121} in the Cu_A domain and the positively charged lysine residues encircling the heme cleft in cytochrome c_{552}. In *T. thermophilus*, on the other hand, the interaction between the corresponding proteins involves mainly hydrophobic and non-ionic contacts (18, 20),

* This work was supported in part by the Deutsche Forschungsgemeinschaft (SFB 472). The costs of publication of this article were defrayed in part by the payment of page charges. This article must therefore be hereby marked "*advertisement*" in accordance with 18 U.S.C. Section 1734 solely to indicate this fact.

◆ This article was selected as a Paper of the Week.

[S] The on-line version of this article (available at http://www.jbc.org) contains supplemental Figs. S1–S3.

The atomic coordinates (code 2FWL) have been deposited in the Protein Data Bank, Research Collaboratory for Structural Bioinformatics, Rutgers University, New Brunswick, NJ (http://www.rcsb.org/).

The ^{1}H and ^{15}N chemical shifts have been deposited in the BioMagResBank data base (http://www.bmrb.wisc.edu) under accession numbers 5819 and 6965 (reduced and oxidized Cu_A domain, respectively) as well as 6966 and 6967 (reduced and oxidized cytochrome c_{552}, respectively).

[1] Supported by the Ministry of Higher Education, Science and Technology (Slovenia).

[2] Present address: Sanofi-Aventis Deutschland GmbH, Industriepark Höchst H780, D-65926 Frankfurt am Main, Germany.

[3] Present address: Dept. for NMR-based Structural Biology, Max Planck Institute for Biophysical Chemistry, Am Fassberg 11, D-37077 Göttingen, Germany.

[4] To whom correspondence should be addressed: Max Planck Research Unit for Enzymology of Protein Folding, Weinbergweg 22, D-06120 Halle (Saale), Germany. Tel.: 49-345-5522819; Fax: 49-345-5511972; E-mail: luecke@enzyme-halle.mpg.de.

possibly because the electrostatic attractions would rather be weakened at the high temperatures these bacteria are exposed to. This different specificity between the reaction partners is also supported by the fact that cytochrome c_{552} from *P. denitrificans* does not interact with the Cu_A domain of *T. thermophilus* (18).

Under steady-state turnover conditions at 25 °C, molar redox activities with $k_{max} = 250\ s^{-1}$ have been reported between cytochrome c_{552} and the ba_3 oxidase of *T. thermophilus* (5). The complex therefore has to be short lived to ensure efficient electron transport (ET).[5] This transient nature of the redox interaction precludes the detection of any intermolecular NOE connectivities to define the contact region between the proteins. However, the highly sensitive amide resonances allow the observation of chemical shift changes as a result of transient alterations in the local environment due to the presence of the redox partner, as previously demonstrated with other systems such as plastocyanin/cytochrome *c*, plastocyanin/cytochrome *f*, cytochrome *c* peroxidase/iso-1-cytochrome *c*, and Cu_A domain/cytochrome c_{552} from *P. denitrificans* for example (19, 21–23).

We therefore employed two isolated, soluble components, *i.e.* cytochrome c_{552} and the Cu_A domain, to determine the biologically relevant ET complex of the *T. thermophilus* system. Contrary to the Cu_A domain from *P. denitrificans*, which was not sufficiently stable for prolonged NMR data collection at room temperature, the Cu_A domain from *T. thermophilus* proved highly stable. Both proteins were complexed under uniform redox conditions that precluded ET; but the transient complex interaction apparently still took place, as in the *P. denitrificans* system (19). Interestingly, analogous to the previous *P. denitrificans* study, in the case of reduced cytochrome c_{552} from *T. thermophilus* we again detected the most pronounced shifts at residues located in the protein interior behind the heme ring. These indirect effects are an indication for redox state-dependent alterations of the electron delocalization in the porphyrin system. Based on chemical shift perturbation mapping, protein-protein docking calculations subsequently yielded the first structural characterization of the ET complex between cytochrome c_{552} and the Cu_A domain that is founded on experimental data. Using this information, the shortest ET pathway from the heme iron to the Cu_A center was calculated based on the "pathway model," revealing an involvement of Phe^{88}, which however does not play such a crucial role as the corresponding Trp^{121} residue in the *P. denitrificans* system (24). Two alternative ET scenarios, matching our experimental mutagenesis data, will be discussed.

EXPERIMENTAL PROCEDURES

Sample Preparation—Cytochrome c_{552} (133 amino acid residues; 14,405 Da including the heme cofactor) and the Cu_A domain (136 residues; 15,062 Da including the two copper atoms) of *T. thermophilus* were both expressed heterologously in *Escherichia coli* and subsequently purified as described previously (18, 25). For ^{15}N enrichment, both proteins were expressed in M9 medium. In the case of cytochrome c_{552}, heme maturation was achieved by co-transformation of the *E. coli* cells with the *ccm*ABCDEFGH gene cluster (26) present on the pEC86 plasmid. Copper atoms were introduced into the apo-Cu_A domain by addition of $Cu(His)_2$ after cell lysis. The NMR resonance assignments revealed that the soluble cytochrome c_{552} protein carried an alanine-to-threonine point mutation in position 123; subsequent activity tests, however, showed the same functionality as the wild-type protein. The Cu_A domain, the water-soluble fragment of the ba_3 oxidase, also was fully functional as revealed by redox spectroscopy (18).

Mutations were introduced by the "altered sites" protocol (Promega, Heidelberg, Germany) as described previously (24). All stopped-flow experiments were carried out in 20 mM BisTris buffer (pH 7.0; 10 mM KCl) at 20 °C, as described elsewhere (18).

For the resonance assignments, NMR samples of 2 mM protein concentration were prepared for each redox partner, containing 20 mM potassium phosphate buffer (pH 6.0), 0.15 mM 2,2-dimethyl-2-silapentane-5-sulfonate (DSS) as internal chemical shift reference (Cambridge Isotope Laboratories, Andover, MA) and 5% D_2O. Depending on the redox state to be investigated, 5 mM sodium ascorbate or 5 mM potassium hexacyanoferrate(III) were added to obtain a fully reduced or oxidized sample, respectively.

For the chemical shift perturbation study, the protein samples were prepared according to the following procedures: 1) two samples both containing 0.5 mM ^{15}N-labeled cytochrome c_{552} in 20 mM potassium phosphate buffer (pH 6.0), 0.15 mM DSS, and 5% D_2O were treated in parallel. Non-labeled Cu_A was added in 4-fold molar excess to one of the two samples. The pH values of both samples were adjusted precisely. To obtain cytochrome c_{552} sample pairs under reduced or oxidized conditions, the solutions included 4 mM sodium ascorbate or 5 mM potassium hexacyanoferrate(III), respectively. 2) Two samples both containing 0.5 mM ^{15}N-labeled Cu_A fragment in 20 mM potassium phosphate buffer (pH 6.0), 0.15 mM DSS, and 5% D_2O were treated likewise. Non-labeled cytochrome c_{552} was added in 4-fold excess to only one of the two samples and pH values checked for both solutions. To obtain Cu_A domain sample pairs under reduced or oxidized conditions, the solutions included 4 mM sodium ascorbate or 5 mM potassium hexacyanoferrate(III), respectively.

NMR Experiments and Analysis—For the resonance assignments of both proteins, NMR spectra were acquired at 25 °C using Bruker DMX 500 and DMX 600 spectrometers operating at 500.13 and 600.13 MHz proton resonance frequencies, respectively, and both equipped with 5-mm triple-resonance $^1H\{^{13}C/^{15}N\}$ probes that have XYZ-gradient capability. The following spectra were collected to assign the resonances of cytochrome c_{552} and the Cu_A domain in both redox states, as described previously (27): two-dimensional $[^1H,^1H]$TOCSY, two-dimensional $[^1H,^1H]$NOESY, two-dimensional $[^{15}N,^1H]$TROSY (28), three-dimensional TOCSY-$[^{15}N,^1H]$TROSY, and three-dimensional NOESY-$[^{15}N,^1H]$TROSY.

In the homonuclear one- and two-dimensional ^1H experiments, the water signal was suppressed by selective presaturation during the relaxation delay, with the carrier placed in the center of the spectrum on the water resonance. All heteronuclear experiments made use of pulsed field gradients for coherence selection and artifact suppression and utilized gradient sensitivity enhancement schemes (29). Quadrature detection in the indirectly detected dimensions was obtained either by the States-TPPI (time proportional phase incrementation) or by the echo/antiecho method. All NMR spectra were acquired and processed on Silicon Graphics computers using the program XWINNMR 3.5 (Bruker Bio-Spin, Rheinstetten, Germany). A 90° phase-shifted squared sine-bell function was used for apodization in all dimensions. Polynomial base-line correction was applied to the processed spectra in the directly detected ^1H dimension. Peak picking and data analysis of the transformed spectra were performed using the AURELIA 2.5.9 (Bruker Bio-Spin) software package. The chemical shifts were referenced to internal DSS to ensure consistency among all spectra (30).

[5] The abbreviations used are: ET, electron transfer; AIR, ambiguous interaction restraint; DSS, 2,2-dimethyl-2-silapentane-5-sulfonate; NOE, nuclear Overhauser effect; NOESY, nuclear overhauser and exchange spectroscopy; TOCSY, total correlation spectroscopy; TROSY, transverse relaxation optimized spectroscopy; PDB, Protein Data Bank; BisTris, 2-[bis(2-hydroxyethyl)amino]-2-(hydroxymethyl)propane-1,3-diol; r.m.s.d., root mean square deviation.

For the chemical shift perturbation mapping, two-dimensional [^{15}N,^{1}H]TROSY spectra were recorded, as described previously (19), at 25 °C and pH 6 on a Bruker Avance 900 spectrometer, operating at 900.13 MHz proton resonance frequency and equipped with a 5 mm cryogenic *z*-gradient ^{1}H{^{13}C/^{15}N} triple-resonance probe. Data acquisition and processing were performed as described above. The backbone amide peaks were picked with the program FELIX 2000 (Accelrys Inc., San Diego, CA). Chemical shift differences in the amide proton ($\Delta\delta_{1HN}$) and nitrogen ($\Delta\delta_{15N}$) resonances of the free and complexed protein forms were combined for each residue by using the expression $[(\Delta\delta_{1HN})^2 + (\Delta\delta_{15N}/6.5)^2]^{1/2}$ (31). These combined chemical shift differences were illustrated with the program MOLMOL (32) by color-coding each respective surface residue.

Docking Calculations—The structure of the cytochrome c_{552}·Cu_A domain complex was determined with the program HADDOCK (high ambiguity driven protein-protein docking) (33) that has been implemented in the program CNS (34), making use of python scripts derived from ARIA (35) for automation. HADDOCK employs biophysical interaction data, such as chemical shift perturbation resulting from NMR titration experiments, that are introduced into the structure calculation as ambiguous interaction restraints (AIRs) to drive the docking process. In our application, four independent sets of amide proton chemical shift perturbation data were available: ^{15}N-labeled cytochrome c_{552} titrated with non-labeled Cu_A domain, both in the reduced and oxidized state, and ^{15}N-labeled Cu_A domain titrated with non-labeled cytochrome c_{552}, again both in the reduced and oxidized state. From each independent data set, the residues with the strongest chemical shift perturbations were selected as "active AIRs" for the HADDOCK calculations; residues with less than 20% accessible surface area, however, were rejected. In addition, surface residues located next to the selected active AIRs were chosen as "passive AIRs", if their relative surface accessibility was also above 20%. The x-ray coordinates of cytochrome c_{552} (PDB ID code 1DT1) and the ba_3 oxidase (PDB ID code 1EHK) were used both to calculate the surface accessibilities with the program NACCESS (36) and for the subsequent docking calculations.

First, 100 structures of the cytochrome c_{552}·Cu_A domain complex were calculated using the rigid docking protocol of HADDOCK. Next, the 20 structures showing the lowest AIR violations were further energy minimized with the side chains of the active and passive residues left flexible. Finally, the 10 best structures were minimized once more in a 8 Å shell of explicit TIP3P (37) water molecules (for details, see Ref. 33). AIR violations, interaction energies, and buried surface areas of the final structures were compared. In addition, the complexes were characterized in terms of electron transfer by the evaluation of electron-tunneling coupling factors using the program GREENPATH (38). In the latter program, the highly interconnected network of bonded and non-bonded contacts within the protein matrix is searched to specify the pathways that maximize the electron-tunneling coupling between the electron donor and acceptor (*i.e.* the iron atom of the cytochrome c_{552} heme moiety and the copper center of the Cu_A domain, respectively). This is achieved using the theories and methods developed by Beratan, Onuchic, and Betts (39), which quantify the ET (without interference) using the pathway model. A pathway is defined as a combination of interacting atoms that link the donor with the acceptor via covalent bonds, hydrogen bonds, and through-space jumps. Rates of non-adiabatic ET reactions can be defined by the expression $k_{ET} = (2\pi/\hbar)|T_{DA}|^2(FC)$. Thereby, the term T_{DA} describes the donor-acceptor interaction associated with electron tunneling, while the FC (Franck-Condon) term contains the free energy dependence (reorganization and reaction free energy) related to nuclear motion.

RESULTS AND DISCUSSION

To allow chemical shift perturbation mapping, the full set of backbone amide resonance values had to be determined for both proteins, *i.e.* cytochrome c_{552} and the Cu_A domain from *T. thermophilus*. The resonance assignments were performed according to the classical strategy based on NOE connectivities between adjacent residues (40), with ^{15}N labeling used to achieve a better signal dispersion. The resulting ^{1}H and ^{15}N assignments of cytochrome c_{552} and the Cu_A domain in both redox states have been deposited at the BioMagResBank data base.

Both redox partners investigated in this study had been shown earlier to be fully functional when expressed in a heterologous host organism (18). Moreover, the *T. thermophilus* proteins, in particular the Cu_A domain, displayed a higher stability compared to the homologous proteins from *P. denitrificans*, which had been employed in an earlier NMR study (19).

NMR Resonance Assignments—The reduced (*i.e.* diamagnetic) cytochrome c_{552} was fully assigned (BMRB-6966); heme proton resonances were determined based on NOE data that agreed with interproton distances in the x-ray structure (PDB ID code 1DT1). Several residues showed highly unusual chemical shift resonances because of ring-current effects; the backbone amide proton resonance of Leu^{116}, for example, is located upfield of the water signal at 4.35 ppm (Fig. 1). The oxidized (*i.e.* paramagnetic) cytochrome c_{552} was assigned nearly completely (BMRB-6967), except for the heme ring and three protein residues: His^{15} and Met^{69}, the two axial ligands of the iron atom, and Cys^{14}, which is bound covalently to the heme ring. Only a few of the heme proton resonances could be identified by using NOE information from the two-dimensional and three-dimensional NOESY data. Certain resonances showed strong line broadening due to the proximity of the paramagnetic center.

The reduced (*i.e.* diamagnetic) Cu_A domain had been previously assigned using triple-resonance experiments (25); however, several aromatic ring proton resonances have been additionally identified in the present work based on homonuclear two-dimensional TOCSY and NOESY spectra (update of BMRB-5819). Interestingly, the ^{1}H resonances of the Phe^{88} ring, which is situated close to the Cu_A center and has been postulated to play a role in the ET (13), were the only aromatic ring resonances that could not be identified. In the case of the oxidized (*i.e.* paramagnetic) Cu_A domain, the assignment of the ^{1}H and ^{15}N resonances was again not complete (BMRB-6965), due to the paramagnetic Cu_A center. Moreover, as reported elsewhere (41), several resonances are extremely shifted, such as an amide group at 300 ppm and certain Cβ protons at 30 ppm. Nevertheless, except for 9 residues (*i.e.* the three N-terminal amino acids Met^{33}–Tyr^{35}, Gly^{115}, and Cys^{149}–Cys^{153}), all other backbone amide groups could be identified for the oxidized Cu_A domain.

Chemical Shift Perturbation Mapping—To obtain structural data on the transient complex between cytochrome c_{552} and the Cu_A domain, two-dimensional [^{15}N,^{1}H]TROSY spectra comparing the free and the complexed state of each protein were collected. Employing ^{15}N-labeled protein samples, the chemical shift changes upon addition of 4-fold molar excess of the non-labeled reaction partner provided crucial information about the residues that are affected by the formation of the complex. The non-labeled redox partner was always added in excess, to shift the equilibrium toward the associated complex state. Nevertheless, the observed effects were rather small, presumably due to the very short-lived nature of the cytochrome c_{552}·Cu_A domain complex. The

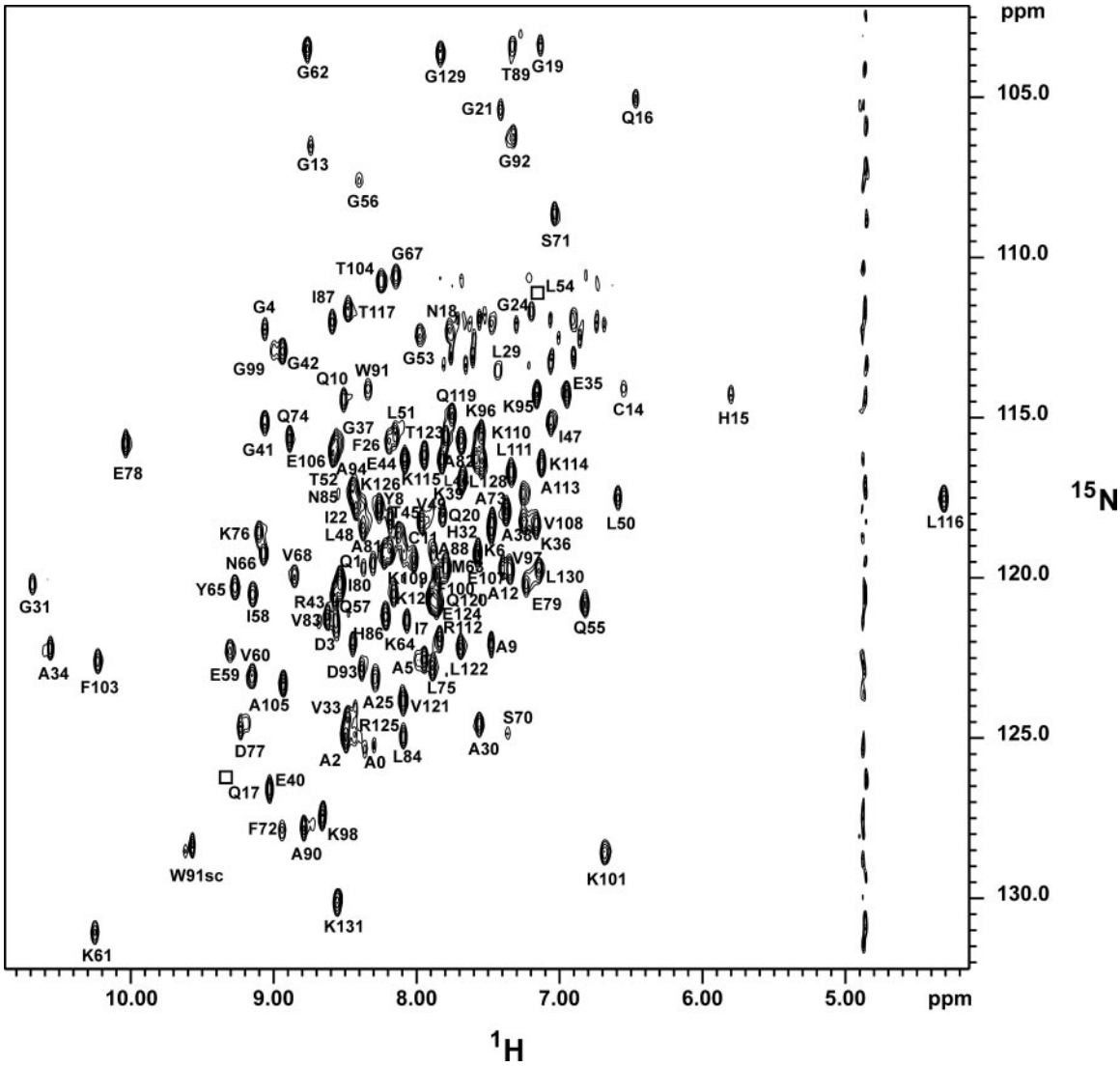

FIGURE 1. **Two-dimensional [^{15}N,^{1}H]TROSY spectrum of cytochrome c_{552} from *T. thermophilus* in the reduced state at pH 6 and 25 °C (^{1}H resonance frequency of 600.13 MHz).** The sequence-specific assignment of the backbone amide resonances is indicated.

chemical shift changes in the ^{1}H and ^{15}N dimensions between the free and complexed protein form were subsequently combined for each residue (31), as indicated in Fig. 2.

In the case of cytochrome c_{552}, for both redox states the most pronounced shift perturbations upon addition of the Cu_A domain were seen in residues located around the heme cleft (Fig. 3), indicating that the "front side" of the protein is the contact surface during the interaction with the redox partner, similar to the corresponding *P. denitrificans* system (19). Moreover, also analogous to the effects noted for *P. denitrificans*, the largest shifts in the reduced state of cytochrome c_{552} from *T. thermophilus* were observed on the back side of the heme cleft, at residues Ala^{34} and His^{32} (Fig. 4); since both residues are not exposed at the protein surface, these dominant shifts must be indirect effects that are apparently relayed from the contact surface through the heme pocket. Interestingly, these indirect effects (at Ala^{34} and His^{32} in *T. thermophilus* and at Gly^{54}, Gly^{55}, and Asp^{56} in *P. denitrificans*) stand out only in the reduced but not in the oxidized state of cytochrome c_{552}. This finding suggests that these chemical shift perturbations in the back of the heme moiety are a result of the electronic differences between the two redox states. More precisely, His^{32} and Arg^{125} form a hydrogen bonding network with the propionate A chain at the back of the heme ring (Fig. 5, *bottom*), resembling the arrangement of Trp^{57}, Arg^{36}, and propionate A in the *P. denitrificans* system (Fig. 5, *top*). We therefore propose that the electronic state of the heme is propagated through the propionate A substituent and across the hydrogen bond to the aromatic ring, *i.e.* His^{32} in *T. thermophilus* or Trp^{57} in *P. denitrificans*. In the case of *P. denitrificans*, for example, fluorescence spectra of reduced and oxidized cytochrome c_{552} (see Fig. S1 in the supplemental data) had shown a 20-nm shift of the tryptophan band (42). This is apparently due to an alteration in the electronic structure of Trp^{57}, since the protein conformation is identical in both redox states as confirmed by both x-ray and NMR structure analysis (42, 43), thus excluding an explanation that is based on conformational changes in the protein structure. Hence, the only distinction that could explain this redox state-dependent effect in the fluorescence spectrum of *P. denitrificans* cytochrome c_{552} is the additional electron delocalized across the porphyrin system. This is a clear indication that the electronic state of the heme system is also sensed in the protein region located beyond the propionate groups. Presumably, the electrons of the heme iron show an effective delocalization toward the periphery of the porphyrin ring including its substituents, as previ-

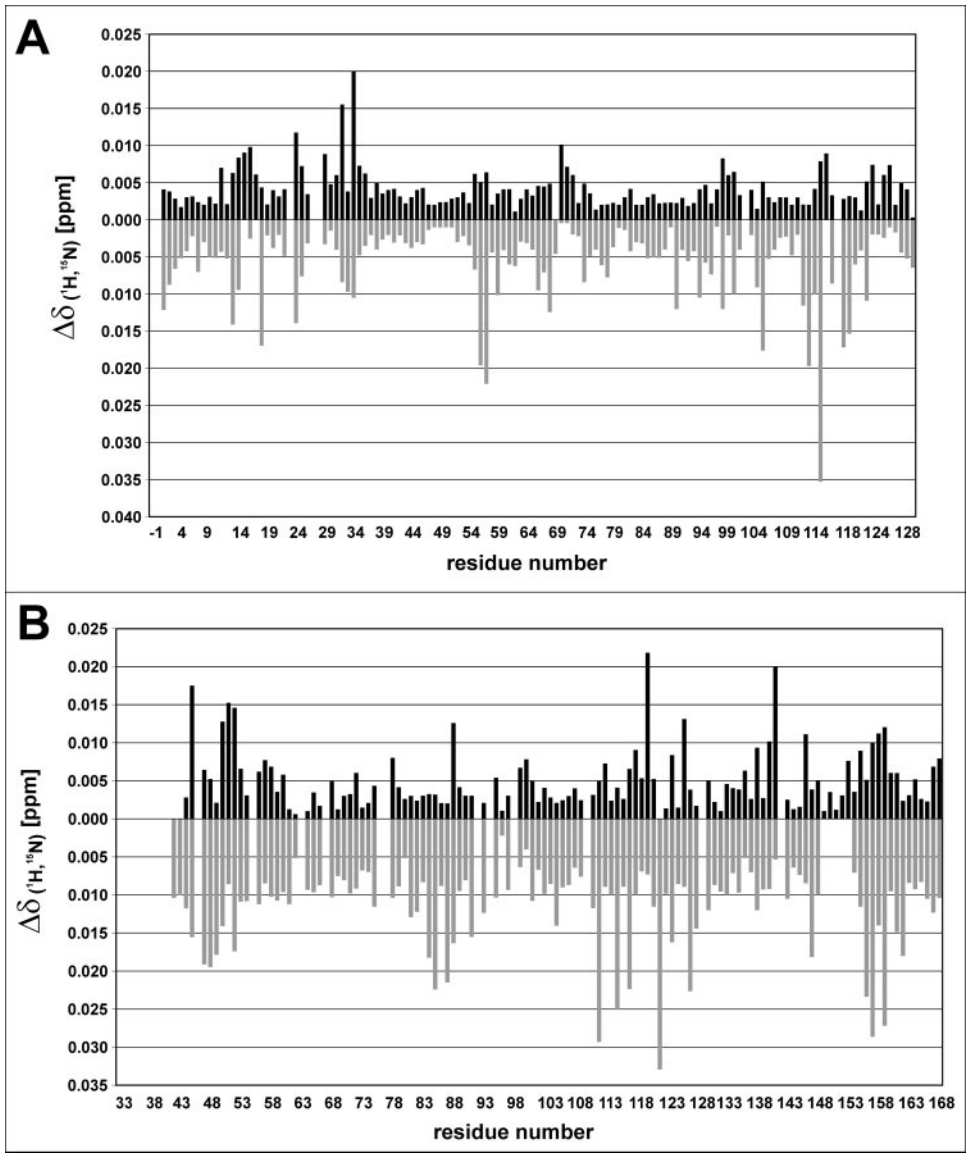

FIGURE 2. **Overview of the combined backbone amide ^1H and ^{15}N chemical shift changes ($\Delta\delta$) that were observed for ^{15}N-labeled cytochrome c_{552} upon addition of 4-fold molar excess Cu_A (*A*) and for ^{15}N-labeled Cu_A upon addition of 4-fold molar excess cytochrome c_{552} (*B*).** *Black bars* (above the base line) indicate shift perturbations in the reduced state, whereas *gray bars* (below the base line) represent the oxidized state.

ously suggested by Johansson *et al.* (44, 45): the actual change of the central iron charge in the redox reaction is only about 0.1–0.2 electrons, despite the unit difference in the formal oxidation state. This relatively small difference in electron probability at the heme iron implies a considerable electron delocalization into the periphery of the porphyrin system, which seems to be very important for both the ET rates and the accommodation of the charged heme moiety in a low dielectric enviroment such as the interior of a protein (44, 45). In our chemical shift perturbation study, the reduced cytochrome c_{552} is additionally complexed with the reduced Cu_A domain. Hence, the electron delocalization in the heme porphyrin ring of the protein complex may be distributed even further into the back of the heme pocket, to minimize unfavorable Coulomb interactions that arise because of increased electron repulsion in the combined heme-Cu_A system, as both redox centers are fully occupied with electrons. This shift in the electron density upon complex formation apparently is sensed by the ring systems of Trp^{57} in *P. denitrifians* or His^{32} in *T. thermophilus* via the hydrogen bond connection to propionate A, thereby in turn presumably affecting their respective local environments (see Fig. 5).

In case of the Cu_A domain, the most pronounced shift perturbations upon addition of cytochrome c_{552} occurred in different regions (Fig. 6). For the docking calculations, however, several of the affected residues could be excluded because of either low surface accessibility or location at the interface to subunit I of the ba_3 oxidase, as described below. The contact region relevant for the ET is located near the Cu_A center, at the surface residues Ala^{87}, Phe^{88}, Gln^{158}, and Asn^{159}.

Theoretically, in the fully oxidized state pseudocontact shifts (see Ref. 46 and references therein) could occur in residues of cytochrome c_{552} that are closest to the paramagnetic copper center of the Cu_A domain, and vice versa; such shifts, however, would hardly be distinguishable from those due to "true" intermolecular contacts. They would arise at the interface between the copper and iron metal centers where most of the intermolecular contacts occur, and thus both effects on the chemical shift would superpose. The impact on the structure calculation using AIRs would therefore be negligible, as indicated also by the consistency of our calculations (see below).

Docking Calculations—To perform docking calculations between cytochrome c_{552} and the Cu_A domain, it was necessary to make a reasonable selection among the residues affected in the chemical shift per-

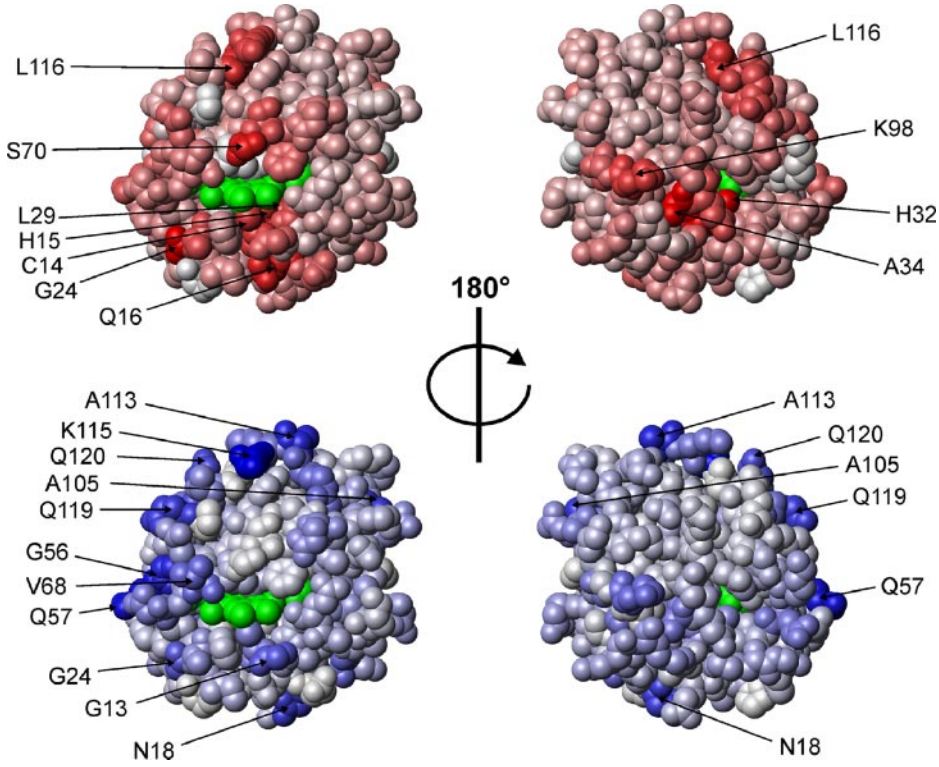

FIGURE 3. **Cytochrome c_{552} structure (PDB ID code 1DT1) color-coded according to the combined backbone amide chemical shift changes ($\Delta\delta$ in Fig. 2*A*), with the color intensity normalized to a maximum of 100% for the residue that was most strongly affected upon complex formation.** The affected residues are shown in *red* for the reduced and in *blue* for the oxidized protein; those residues showing the most pronounced shifts are labeled. For clarity, not just the backbone amides are highlighted but rather the entire residues have been colored. The molecules on the *left* and *right* are rotated by 180° about the *vertical axis* relative to each other. The front side (*left picture*) with the heme (*green*) in the center represents the contact surface in the complex with the Cu_A domain.

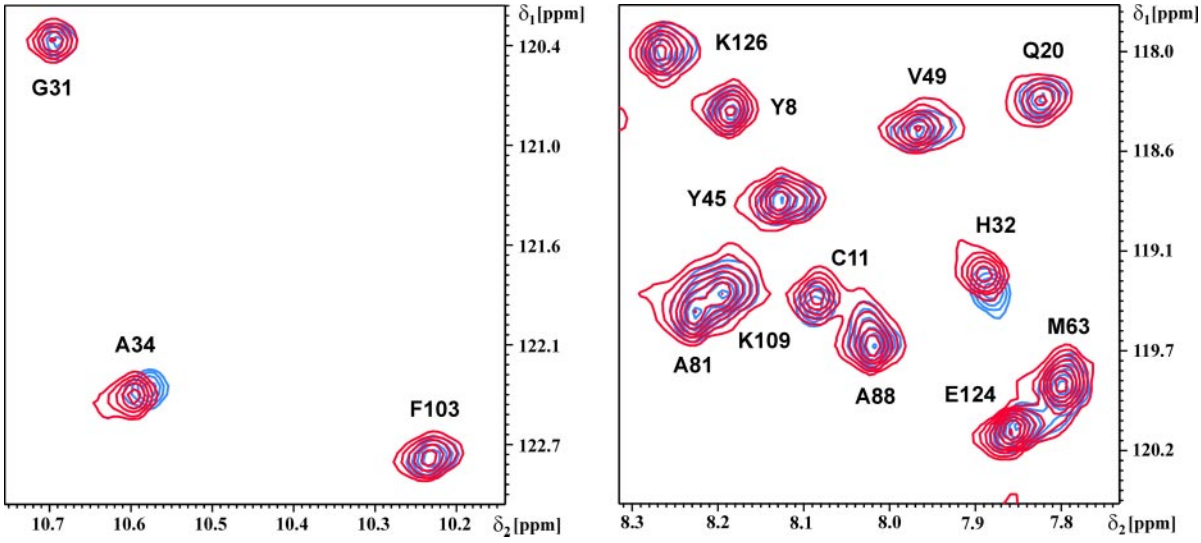

FIGURE 4. **Sections from two-dimensional [^{15}N,^{1}H]TROSY spectra of cytochrome c_{552} in the reduced state at pH 6 and 25 °C (^{1}H resonance frequency of 900.13 MHz).** Differences in the superpositions of cytochrome c_{552} resonances between the free (*red*) and complexed (*blue*) protein are only minute due to the transient nature of complex formation. The largest shifts were detected for two residues located in the protein interior, Ala^{34} and His^{32}, thus implying that these are indirect effects.

turbation experiments, based on their surface accessibility and location in the molecule relative to the redox center.

In the case of reduced cytochrome c_{552}, residues Ala^{34}, His^{32}, Gly^{24}, Ser^{70}, Gln^{16}, His^{15}, Leu^{116}, Leu^{29}, Cys^{14}, and Lys^{98} (in this order) showed the largest combined chemical shift perturbations ($\Delta\delta \geq 0.008$ ppm). Some of these residues were excluded as possible contact partners for the following reasons: Ala^{34}, His^{32}, His^{15}, Leu^{116}, Leu^{29}, and Cys^{14} were rejected because of a too low surface accessibility (<20%); Lys^{98} could be neglected due to its location on the back side of the molecule. Thus, residues Gly^{24} and Ser^{70} (both with over 40% relative surface accessibility) were chosen as active AIRs, whereas Gln^{16} with only 28.7% relative surface accessibility was classified as passive AIR.

In the oxidized cytochrome c_{552}, residues Lys^{115}, Gln^{57}, Ala^{113}, Gly^{56}, Ala^{105}, Gln^{119}, Asn^{18}, Gln^{120}, Gly^{13}, Gly^{24}, and Val^{68} (in this order) showed the largest combined chemical shift perturbations ($\Delta\delta \geq 0.0124$ ppm). Ala^{105} was excluded because of its posititon on the back side of the molecule. Gly^{56} (with 23.4% relative surface accessibility) was classified as passive AIR. All the other affected residues show over 40% relative surface accessibility and were therefore accepted as active AIRs.

In the case of the reduced Cu_A domain, residues Gly^{120}, Arg^{141}, Ile^{45}, Glu^{51}, Arg^{52}, Glu^{126}, Leu^{50}, Phe^{88}, Asn^{159}, Gln^{158}, Arg^{146}, Lys^{140}, and His^{157} (in this order) showed the largest combined chemical shift perturbations ($\Delta\delta \geq 0.010$ ppm). Gly^{120}, Ile^{45}, and Glu^{126} could be excluded because of their position at the interface to subunit I of the ba_3 oxidase

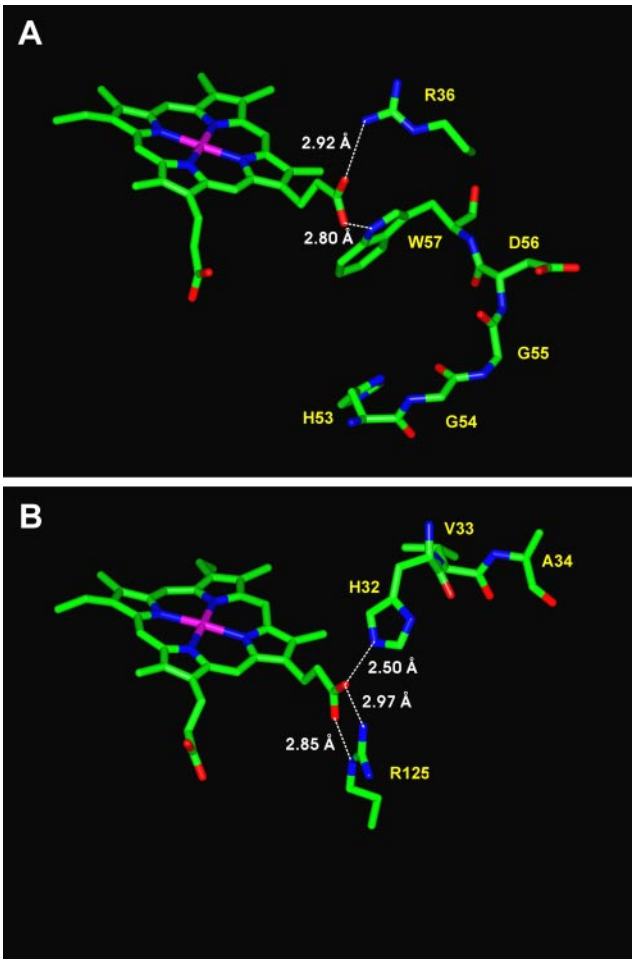

FIGURE 5. **The spatial orientations of the heme moieties in cytochrome c_{552} from *P. denitrificans* (*A*) and *T. thermophilus* (*B*).** In both cases, the carboxylate group of propionate A forms hydrogen bonds to an arginine side chain and an aromatic ring. The amide groups with the largest chemical shift perturbations upon complex formation in the reduced state (*i.e.* Gly^{54}, Gly^{55}, and Asp^{56} in *P. denitrificans*, respectively, His^{32} and Ala^{34} in *T. thermophilus*) are always situated beyond the aromatic ring.

(see Fig. S2 in the supplemental data). Arg^{141}, Arg^{52}, Leu^{50}, and Lys^{140} were also neglected, since these residues are only accessible in the soluble Cu_A fragment, while in the full ba_3 oxidase their side chains should be immersed into the lipid membrane. Glu^{51} was not taken into account, since it is located at the opposite side of the Cu_A domain relative to the copper center. His^{157} and Gln^{158} were rejected because of too low surface accessibilities (<20%). The remaining residues Phe^{88}, Arg^{146}, and Asn^{159} were chosen as active AIRs.

In the oxidized Cu_A domain, residues Asn^{122}, Val^{112}, His^{157}, Asn^{159}, Gly^{115}, Gly^{156}, Val^{127}, Ala^{85}, His^{117}, and Ala^{87} (in this order) showed the largest chemical shift perturbations ($\Delta\delta \geq 0.020$ ppm). Val^{112}, His^{157}, Gly^{115}, Val^{127}, and Ala^{85} could be excluded because of too low surface accessibilities (<20%). Asn^{122} and His^{117} were also neglected because they are located at the interface to subunit I of the ba_3 oxidase. The remaining residues Ala^{87}, Gly^{156}, and Asn^{159} were accepted as active AIRs.

All residues that were thus chosen for the docking calculations as active AIRs (10 and 5 for cytochrome c_{552} and the Cu_A domain, respectively) are listed in Table 1. Consequently, neighboring residues with relative surface accessibility above 20% were selected as passive AIRs for the calculations. Based on these AIRs, 100 rigid structures of the cytochrome c_{552}·Cu_A domain complex were calculated with the HADDOCK program (33). The 20 structures with the lowest interaction energies were further energy minimized by keeping the side chains of the active and passive residues flexible. Finally, the 10 lowest energy structures were minimized once more in a shell of explicit water molecules. Listed in Table 2 are the energy terms, buried surface areas, ET distances, ET pathway lengths, and ET efficiencies of the 10 final structures. The distance between the electron donor (*i.e.* the iron atom of cytochrome c_{552}) and acceptor (*i.e.* the copper atom CU2 of the Cu_A domain) varies between 15.6 and 16.8 Å. The estimated electron-tunneling coupling factor ($\log |T_{DA}^2|$) ranges from −11.2 to −12.8 and the electron pathway length from 19.6 to 24.5 Å. The total interaction energy varies in the ensemble between −124 and −79 kcal/mol.

As the contact surfaces of the protein molecules are rather flat, and since the AIRs allow different contact combinations between the active and passive residues of the two redox partners, no single preferred solu-

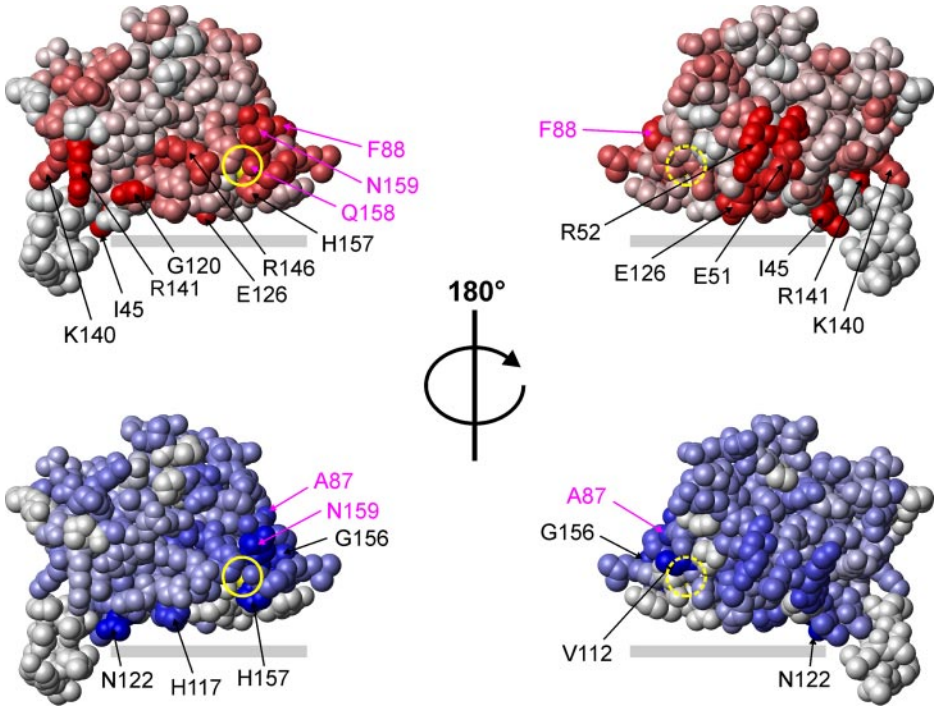

FIGURE 6. **The Cu_A domain structure (PDB ID code 1EHK) is color-coded according to the combined backbone amide chemical shift changes ($\Delta\delta$ in Fig. 2*B*), with the color intensity normalized to a maximum of 100% for the residue that was most strongly affected upon complex formation.** The affected residues are shown in *red* for the reduced and in *blue* for the oxidized protein; those residues showing the most pronounced shifts are labeled. For clarity, not just the backbone amides are highlighted, but rather the entire residues have been colored. Molecules on the *left* and *right* are rotated around the *vertical axis* by 180° relative to each other. The Cu_A domain has a slightly elongated form, with the ET-relevant contact surface located at the end where the side chains of residues Ala^{87}, Phe^{88}, Gln^{158}, and Asn^{159} (*purple arrows*) protrude at the surface close to the mostly occluded Cu_A center (*yellow* atoms marked by a *full circle* in the "front view" or by a *broken circle* in the "back view"). The appendix at the other end denotes the start of the membrane anchor; the Cu_A domain itself rests on the membrane-embedded subunit I, as indicated by the *gray bar*.

TABLE 1

Residues of cytochrome c_{552} and the Cu_A domain used as active and passive AIRs in the docking calculations

Redox partner	Active AIRs	Passive AIRs
Cytochrome c_{552}	Gly^{13}, Asn^{18}, Gly^{24}, Gln^{57}, Val^{68}, Ser^{70}, Ala^{113}, Lys^{115}, Gln^{119}, Gln^{120}	Cys^{11}, Gln^{16}, Gln^{17}, Gln^{20}, Ile^{22}, Pro^{23}, Ala^{25}, Phe^{26}, Gln^{55}, Gly^{56}, Met^{63}, Lys^{64}, Asn^{66}, Gly^{67}, Ser^{71}, Trp^{91}, Lys^{109}, Lys^{110}, Arg^{112}, Lys^{114}, Thr^{117}, Pro^{118}, Thr^{123}, Glu^{124}
Cu_A domain	Ala^{87}, Phe^{88}, Arg^{146}, Gly^{156}, Asn^{159}	Phe^{86}, Glu^{119}, Glu^{144}, Leu^{155}, Phe^{161}

TABLE 2

Properties of the 10 final structures representing the cytochrome c_{552}·Cu_A domain complex, sorted according to the distance between the iron atom of cytochrome c_{552} and the closest copper atom of the Cu_A center (CU2 in all cases)

No.	Distance (FE-CU2)	Intermolecular energy[a]				Buried surface	Electron transfer[b]		r.m.s.d.[c]
		Total	vdw	Elec	AIR		Length	log $\lvert T_{DA}^2 \rvert$	
	Å	kcal/mol				Å²	Å		Å
1	15.59	−102.3	−52.4	−64.4	14.5	1377	19.60	−11.2	NA[d]
2	15.78	−110.0	−59.5	−67.5	17.0	1535	19.55	−11.2	2.31
3	15.87	−123.6	−63.1	−80.3	19.7	1563	19.96	−11.8	4.54
4	16.03	−91.9	−53.9	−56.4	18.3	1602	20.07	−11.9	3.21
5	16.05	−86.1	−44.7	−59.3	17.9	1426	20.34	−12.3	2.34
6	16.18	−98.9	−52.4	−64.8	18.4	1488	22.13	−11.8	1.57
7	16.31	−93.2	−54.3	−53.5	14.6	1314	20.83	−11.7	2.72
8	16.32	−78.3	−55.0	−42.1	18.8	1495	19.96	−11.8	3.33
9	16.61	−92.2	−59.2	−49.6	16.7	1360	20.54	−11.4	3.82
10	16.77	−79.0	−45.2	−52.2	18.3	1354	24.87	−12.8	2.35

[a] The total, van der Waals (vdw), electrostatic (Elec), and AIR energy terms for the intermolecular interaction.
[b] Electron-tunneling coupling factor, log $|T_{DA}|^2$, and electron pathway length of the best pathway found in each structure with the program GREENPATH (38).
[c] r.m.s.d. of the cytochrome c_{552} backbone atoms relative to structure 1, when the Cu_A domain is superposed in all 10 conformers.
[d] Not applicable.

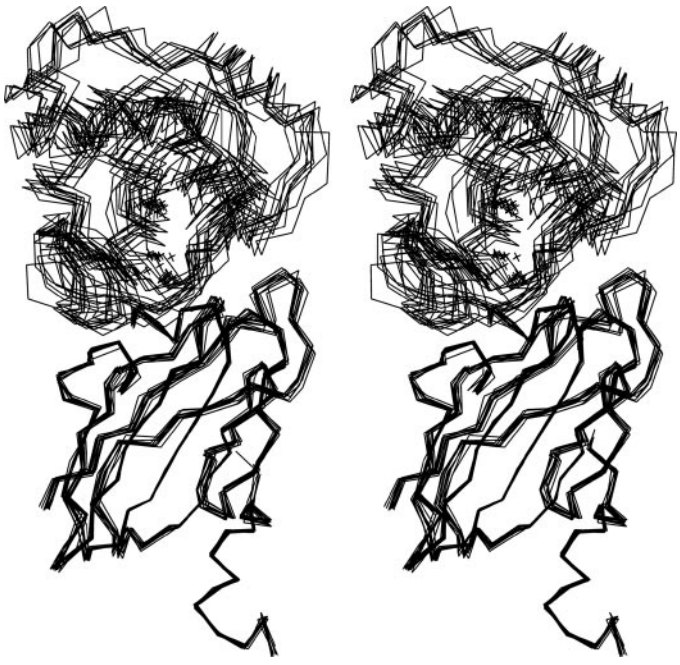

FIGURE 7. **Stereo view of the 10 final structures of the cytochrome c_{552}·Cu_A domain complex, with the backbone atoms of the Cu_A domain superposed on the *bottom*.** The ensemble shows a single structure cluster, whereby the less aligned cytochrome c_{552} conformers still produce very similar docking arrangements with the water-soluble part of subunit II.

tion was expected from these docking calculations (33). In the present work, however, superposition of the Cu_A backbone atoms revealed an ensemble of complex structures where the backbone r.m.s.d. values of the cytochrome c_{552} conformers ranged between 1.57 and 4.54 Å relative to structure 1 (Fig. 7). In other words, the cytochrome c_{552} positions display only a moderate variation, thus indicating that all 10 lowest energy conformers essentially belong to the same complex structure cluster. Structures 1–3 (see Table 2), which display the closest proximity between the electron donor and acceptor atoms (<16 Å), moreover possess the most favorable total interaction energies (<−100 kcal/mol) and exhibit an identical ET pathway; they were therefore selected as most representative of the cytochrome c_{552}·Cu_A domain complex and their atom coordinates deposited at the Brookhaven Data Bank under PDB ID code 2FWL. (The cytochrome c_{552} backbone r.m.s.d. between the superposed complex structures 2 and 3 is 2.55 Å).

None of the calculated complexes was able to fully compensate the potential energy that is associated with the AIRs; its contribution, however, remains significantly smaller than the van der Waals or electrostatic terms. More importantly, intermolecular contacts with the partner molecule were shown either directly by the residues classified as active AIRs or at least by one of the respective neighboring residues representing passive AIRs. The intermolecular contacts in structure 1, as displayed in Fig. 8, are therefore in agreement with the experimental picture; this has been achieved with a set of high-quality AIRs, derived from four independent experiments. Moreover, in agreement with the postulated hydrophobic/non-ionic character of the cytochrome c_{552}·Cu_A domain interaction in the *T. thermophilus* system (18, 20), about 40% of the contact surfaces are composed of hydrophobic residues. This is due to a large number of nonpolar intermolecular interactions (see Fig. 8), for example by Ile^{22} and Val^{68} (both in cytochrome c_{552}) as well as Phe^{88} and Leu^{155} (both in the Cu_A domain), whereas only two charged residues (Lys^{115} in cytochrome c_{552} and Arg^{146} in the Cu_A domain) are found within the protein-protein contact zone, in comparison to an inner ring of four positively charged lysine residues encircling the heme cleft in *P. denitrificans* cytochrome c_{552} (19).

An additional consideration regarding the quality of the complex structures involves the Cu_A domain that was used in the chemical shift perturbation experiments. This Cu_A domain represents merely the solvent-exposed part of the entire ba_3 oxidase. It is reasonable to assume, however, that the complete ba_3 oxidase forms the same type of complex with cytochrome c_{552} like the free Cu_A domain. To test whether this is true for complex structures 1–3, the Cu_A domain coordinates were reattached to subunit I of the ba_3 oxidase (Fig. 9). Subsequent analysis for steric overlap with the corresponding cytochrome c_{552} molecule displayed only few addi-

		cua												
		PHE 86	ALA 87	PHE 88	GLY 89	TYR 90	GLN 91	ASN 93	ARG 146	LEU 155	GLY 156	GLN 158	ASN 159	PHE 161
cyt c_{552}														
GLY	13	1					1							
ILE	22							9						
GLY	24								1					
ALA	25							1						
PHE	26	1			3	1								
GLN	55									2	2	3		
GLY	56												4	
GLN	57												1	
ASN	66								3				3	3
GLY	67												3	
VAL	68			7							5		5	
SER	70		1	3										
SER	71			1										
LYS	115									1				
THR	117									8				
PRO	118									5				
heme			3											

FIGURE 8. **Intermolecular interaction matrix of cytochrome c_{552} (*cyt*c_{552}) and the Cu_A domain (*cua*) in complex structure 1 (see Table 2), showing the number of atom-to-atom contacts closer than 2.8 Å for each residue involved in the complex formation.** This scheme was prepared with the program *nmr2st* (27).

FIGURE 9. **Structural model of the transient redox complex between cytochrome c_{552} and the ba_3 oxidase of *T. thermophilus* based on the energetically best complex structure 1 (see Table 2).** The heme *c* moiety (*orange*) of cytochrome c_{552} (*green ribbon*) approaches the binuclear Cu_A center (*magenta*) of subunit II (*yellow*) for subsequent electron transfer to occur. The electrons are then passed on to the cofactors heme *b* and heme a_3 (both in *red*) and Cu_B (*magenta*) in subunit I (*cyan*; residues 496–500 in the loop between transmembrane helices 12 and 13 are missing in the x-ray structure). Subunit IIa is colored in *blue*. This picture was created with the program GRASP (54).

tional close contacts, mainly between the side chains of Gln^{455} (subunit I) and Gln^{119} (cytochrome c_{552}) in structures 1 and 2 and between Trp^{559} (subunit I) and Gln^{57} (cytochrome c_{552}) in structure 3. However, no backbone-to-backbone contacts occurred in any of these cases. The same type of complex as obtained in structures 1–3 can thus be formed *in vivo* by cytochrome c_{552} and the complete ba_3 oxidase.

The Electron Pathway—The program GREENPATH (38) was used to compare, based on the pathway model, the ET efficiencies within the complex structures by calculating the electron-tunneling coupling factors. The Franck-Condon term (see "Experimental Procedures") contains the free energy dependence related to nuclear motion; this is difficult to quantify, since it requires the evaluation of reorganization energies, but should be approximately constant for different complex conformations of the same partners. The results obtained with this method have been quite successful in the prediction of ET properties of proteins (see Refs. 47 and 48 and references therein), although the semi-empirical formulation behind it is a simplification of more complete descriptions (49). The shortest electron pathway proposed for the cytochrome c_{552}·Cu_A domain complex was found in structure 1. The electron originates at the porphyrin system in cytochrome c_{552}, formally traveling from the iron center along the heme NC, C4C, C3C, CAC, and CBC atoms, and crosses over to the Ala^{87} backbone oxygen in the Cu_A domain. The electron continues along the Ala^{87}-Phe^{88} peptide bond to the amide proton of Phe^{88}, where another jump occurs to the imidazole ring of His^{114}, a direct ligand of the Cu_A center. Continuing along the His^{114} ring atoms HE1, CE1, and ND1, the electron eventually reaches the copper atom CU2 (Fig. 10).

This pathway involves residues Ala^{87} and Phe^{88} of the Cu_A domain, which both showed significant perturbations of the amide ^1H and ^{15}N chemical shifts upon titration with cytochrome c_{552}. Moreover, the involvement of Phe^{88} in the ET was confirmed by site-directed mutagenesis experiments: replacement of Phe^{88} by a leucine residue did not completely abolish the ET rates in stopped-flow kinetics (see Fig. S3 in the supplemental data) but diminished its efficiency significantly to ~68% of the apparent bimolecular rate constant in the physiological direction compared with the wild-type (WT) protein ($k_{forward}$(WT): $5.0 \times 10^6\ M^{-1}\ s^{-1}$, $k_{forward}$(F88L): $3.4 \times 10^6\ M^{-1}\ s^{-1}$). This situation is different to the *P. denitrificans* system, where the corresponding Trp^{121} residue in the Cu_A domain has a key role in the ET to cytochrome c_{552} (24, 50, 51): substitution of Trp^{121}, *e.g.* by glutamine, rendered the enzyme inactive. The fact that the F88L mutant of *T. thermophilus* still shows 68% ET activity therefore suggests that one or more alternative pathways may exist. The neighboring Phe^{86}, corresponding to Tyr^{122} in *P. denitrificans*, could be excluded as possible ET component for several reasons: first, the F86L mutant was fully functional like the wild-type protein. Second, the F86L/F88L double mutant showed the same reduction in the ET activity as the F88L mutation alone. And finally, the Phe^{86} ring is too far off the line connecting the heme with the Cu_A center to warrant an efficient ET.

As a consequence, the influence of Phe^{88} on the ET can be narrowed down to two possible scenarios. Either the ET pathway proposed by the GREENPATH program is the only biologically relevant route the electron can take, in which case the effect of the F88L mutation on the ET activity must be due to the resulting decrease of the hydrophobic portion in the contact surface and/or changes in the reorganization energy; or as we assume more likely, the electron can principally take two alternative paths both involving position 88 of the Cu_A domain (Fig. 10). The through-bond pathway of ~19–20 Å length, as proposed by GREENPATH, has only short through-space jumps of 1.83 Å (between heme HBC and Ala^{87} O) and 2.95 Å (between Phe^{88} HN and His^{114} HE1). In this case, the closest edge-to-edge distance between the conjugated donor and acceptor systems (*i.e.* the heme ring and the His^{114} imidazole ring, respectively) is 10.9 Å. This distance can be bridged easily and efficiently by a tunneling electron, as the majority of known ET reac-

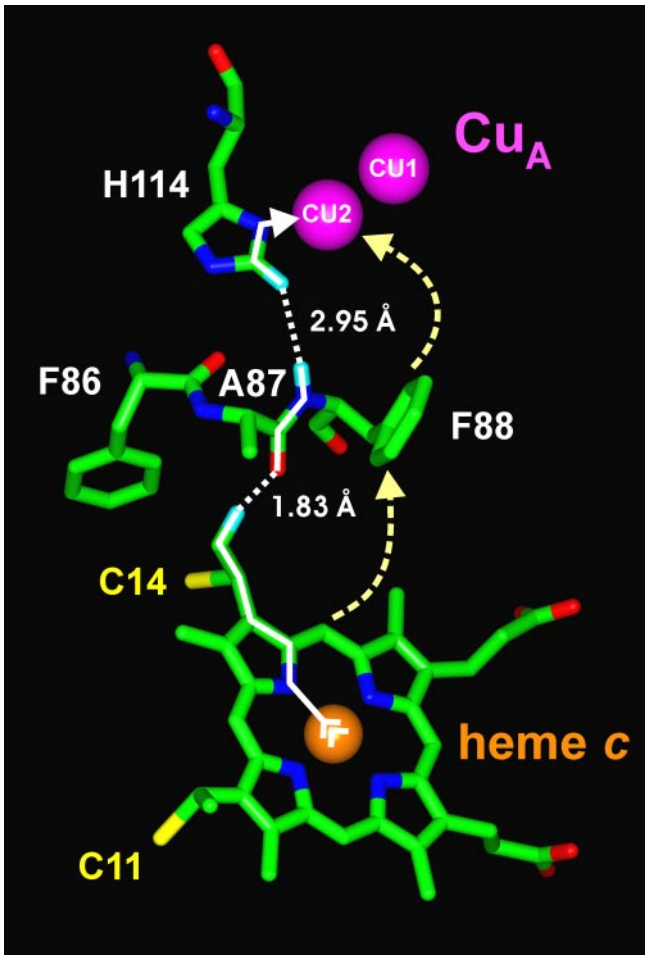

FIGURE 10. **The ET pathways proposed for the cytochrome c_{552}·Cu_A domain complex of *T. thermophilus* based on the energetically best complex structure 1 (see Table 2).** In the through-bond pathway (*white arrow*), the electron travels from the heme of cytochrome c_{552} to Ala^{87}, Phe^{88}, His^{114}, and finally the binuclear copper center of the Cu_A domain; through-space jumps are indicated by *dotted segments* with the jump distances marked. The edge-to-edge distance between the electron donor and acceptor systems (*i.e.* the heme moiety and the His^{114} imidazole ring, respectively) is 10.9 Å. An alternative through-space pathway (*dashed yellow arrows*) could transfer the electron via longer jumps from the heme CHD atom to the Phe^{88} ring (6.9 Å) and onward either to the His^{114} ring (6.4 Å) or directly to the Cu_A center (6.7 Å).

tions between natural redox centers occur over distances of 14 Å or less (52). These ET reactions are remarkably rapid and specific with favorable electron-tunneling coupling factors, since the coupling via covalent bonds and hydrogen bonds is much stronger than that across van der Waals gaps. According to Gray and Winkler (53), in a protein environment electrons will tunnel a distance of ~11 Å on the nanosecond to subnanosecond time scale; hence, it may be concluded that the ET is not the limiting factor in the turnover rate between cytochrome c_{552} and the Cu_A domain from *T. thermophilus*, which typically ranges between 100 and 250 s^{-1} (5).

Alternatively, the electron may also travel from the heme moiety either to the His^{114} imidazole ring or directly to the Cu_A center entirely by through-space jumps via the Phe^{88} ring (see *dashed arrows* in Fig. 10), thereby bridging a total distance of around 13.5 Å. However, in this case the transfer rates should be rather low, as electrons tunnel "through space" from one center to another with a rate that decreases exponentially with distance. Although this edge-to-edge distance is still within the productivity limit for ET through space, it should be less efficient compared with the "through-bond" path outlined above, as indicated by the fact that the F88L mutation reduced the ET activity by not more than 32%.

Hence, both pathways appear possible within biologically relevant time scales according to current ET theories (52, 53). Substitution of the phenyl ring by an aliphatic side chain in the F88L mutant would therefore eliminate only one of the possible ET pathways. In fact, the through bond pathway along the backbone of Ala^{87} and Phe^{88} might even represent a rational solution from an evolutionary point of view, since in this case the ET will not be significantly affected by spontaneous point mutations that could otherwise possibly render the system inactive by eliminating an essential side chain.

Acknowledgments—We thank A. M. J. J. Bonvin (Utrecht University, Utrecht, The Netherlands) for help with the HADDOCK program, T. Soulimane (University of Limerick, Limerick, Ireland) for kindly providing wild-type cytochrome c_{552} and ba_3 oxidase for activity tests, Britta Reincke (University of Frankfurt, Frankfurt, Germany) for the fluorescence spectra of cytochrome c_{552}, and H. W. Müller (University of Frankfurt) for technical assistance.

REFERENCES

1. Oshima, T., and Imahori, K. (1974) *Int. J. Syst. Bacteriol.* **24,** 102–112
2. Williams, R. A. D. (1989) *Microbiology of Extreme Environments and Its Potential for Biotechnology*, pp. 82–97, Elsevier, London, UK
3. Yano, T., Chu, S. S., Sled', V. D., Ohnishi, T., and Yagi, T. (1997) *J. Biol. Chem.* **272,** 4201–4211
4. Mooser, D., Maneg, O., Corvey, C., Steiner, T., Malatesta, F., Karas, M., Soulimane, T., and Ludwig, B. (2005) *Biochim. Biophys. Acta* **1708,** 262–274
5. Soulimane, T., von Walter, M., Hof, P., Than, M., Huber, R., and Buse, G. (1997) *Biochem. Biophys. Res. Commun.* **237,** 572–576
6. Fee, J. A., Choc, M. G., Findling, K. L., Lorence, R., and Yoshida, T. (1980) *Proc. Natl. Acad. Sci. U. S. A.* **77,** 147–151
7. Soulimane, T., Gohlke, U., Huber, R., and Buse, G. (1995) *FEBS Lett.* **368,** 132–134
8. Fee, J. A., Chen, Y., Todaro, T. R., Bren, K. L., Patel, K. M., Hill, M. G., Gomez-Moran, E., Löhr, T. M., Ai, J., Thöny-Meyer, L., Williams, P. A., Stura, E., Sridhar, V., and McRee, D. E. (2000) *Protein Sci.* **9,** 2074–2084
9. Moore, G. R., and Pettigrew, G. W. (1990) *Cytochromes c: Evolutionary, Structural and Physicochemical Aspects*, Springer-Verlag, Berlin
10. Scott, R. A., and Mauk, A. G. (1996) *Cytochrome C, A Multidisciplinary Approach*, University Science Books, Sausalito, CA
11. Williams, P. A., Blackburn, N. J., Sanders, D., Bellamy, H., Stura, E. A., Fee, J. A., and McRee, D. E. (1999) *Nat. Struct. Biol.* **6,** 509–516
12. Bresser, A., and Buse, G. (1993) *Biol. Chem.* **374,** 736
13. Soulimane, T., Buse, G., Bourenkov, G. P., Bartunik, H. D., Huber, R., and Than, M. E. (2000) *EMBO J.* **19,** 1766–1776
14. Kannt, A., Soulimane, T., Buse, G., Becker, A., Bamberg, E., and Michel, H. (1998) *FEBS Lett.* **434,** 17–22
15. Zimmermann, B., Nitsche, C., Fee, J., Rusnak, F., and Munck, E. (1988) *Proc. Natl. Acad. Sci. U. S. A.* **85,** 5779–5783
16. Antholine, W., Kastrau, D., Steffens, G., Buse, G., Zumft, W., and Kroneck, P. (1992) *Eur. J. Biochem.* **209,** 875–881
17. Kelly, M., Lappalainen, P., Talbo, G., Haltis, T., van der Oost, J., and Saraste, M. (1993) *J. Biol. Chem.* **268,** 16781–16787
18. Maneg, O., Ludwig, B., and Malatesta, F. (2003) *J. Biol. Chem.* **278,** 46734–46740
19. Wienk, H., Maneg, O., Lücke, C., Pristovšek, P., Löhr, F., Ludwig, B., and Rüterjans, H. (2003) *Biochemistry* **42,** 6005–6012
20. Maneg, O., Malatesta, F., Ludwig, B., and Drosou, V. (2004) *Biochim. Biophys. Acta* **1655,** 274–281
21. Ubbink, M., and Bendall, D. S. (1997) *Biochemistry* **36,** 6326–6335
22. Worrall, J. A., Kolczak, U., Canters, G. W., and Ubbink, M. (2001) *Biochemistry* **40,** 7069–7076
23. Díaz-Moreno, I., Díaz-Quintana, A., De la Rosa, M. A., and Ubbink, M. (2005) *J. Biol. Chem.* **280,** 18908–18915
24. Witt, H., Malatesta, F., Nicoletti, F., Brunori, M., and Ludwig, B. (1998) *J. Biol. Chem.* **273,** 5132–5136
25. Mukrasch, M. D., Lücke, C., Löhr, F., Maneg, O., Ludwig, B., and Rüterjans, H. (2004) *J. Biomol. NMR* **28,** 297–298
26. Thöny-Meyer, L., Fischer, F., Künzler, P., Ritz, D., and Hennecke, H. (1995) *J. Bacteriol.* **177,** 4321–4326
27. Pristovšek, P., Lücke, C., Reincke, B., Ludwig, B., and Rüterjans, H. (2000) *Eur. J. Biochem.* **267,** 4205–4210

28. Pervushin, K., Riek, R., Wider, G., and Wüthrich, K. (1997) *Proc. Natl. Acad. Sci. U. S. A.* **94,** 12366–12371
29. Muhandiram, D. R., and Kay, L. E. (1994) *J. Magn. Reson. Ser. B* **103,** 203–216
30. Wishart, D. S., Bigam, C. G., Yao, J., Abildgaard, F., Dyson, H. J., Oldfield, E., Markley, J. L., and Sykes, B. D. (1995) *J. Biomol. NMR* **6,** 135–140
31. Mulder, F. A., Schipper, D., Bott, R., and Boelens, R. (1999) *J. Mol. Biol.* **292,** 111–123
32. Koradi, R., Billeter, M., and Wüthrich, K. (1996) *J. Mol. Graphics* **41,** 51–55
33. Dominguez, C., Boelens, R., and Bonvin, A. M. (2003) *J. Am. Chem. Soc.* **125,** 1731–1737
34. Brunger, A. T., Adams, P. D., Clore, G. M., DeLano, W. L., Gros, P., Grosse-Kunstleve, R. W., Jiang, J. S., Kuszewski, J., Nilges, J., Pannu, N. S., Read, R. J., Rice, L. M., Simonson, T., and Warren, G. L. (1998) *Acta Crystallogr. Sect. D Biol. Crystallogr.* **54**, 905–921
35. Linge, J. P., O'Donoghue, S. I., and Nilges, M. (2001) *Methods Enzymol.* **339,** 71–90
36. Hubbard, S. J., and Thornton, J. M. (1993) *NACCESS Computer Program*, Department of Biochemistry and Molecular Biology, University College London, London, UK
37. Jorgensen, W. L., Chandrasekhar, J., Madura, J. D., Impey, R. W., and Klein, M. L. (1983) *J. Chem. Phys.* **79,** 926–935
38. Regan, J. J., Risser, S. M., Beratan, D. N., and Onuchic, J. N. (1993) *J. Phys. Chem.* **97,** 13083–13088
39. Beratan, D. N., Betts, J. N., and Onuchic, J. N. (1991) *Science* **252,** 1285–1288
40. Wüthrich, K. (1986) *NMR of Proteins and Nucleic Acids*, Wiley, New York
41. Bertini, I., Bren, K., Clemente, A., Fee, J. A., Gray, H. B., Luchinat, C., Malmström, B. G., Richards, J. H., Sanders, D., and Slutter, C. E. (1996) *J. Am. Chem. Soc.* **118,** 11658–11659
42. Reincke, B., Perez, C., Pristovšek, P., Lücke, C., Ludwig, C., Löhr, F., Rogov, V. V., Ludwig, B., and Rüterjans, H. (2001) *Biochemistry* **40,** 12312–12320
43. Harrenga, A., Reincke, B., Rüterjans, H., Ludwig, B., and Michel, H. (2000) *J. Mol. Biol.* **295,** 667–678
44. Johansson, M. P., Sundholm, D., Gerfen, G., and Wikström, M. (2002) *J. Am. Chem. Soc.* **124**, 11771–11780
45. Johansson, M. P., Blomberg, M. R., Sundholm, D., and Wikström, M. (2002) *Biochim. Biophys. Acta* **1553,** 183–187
46. Bertini, I., Luchinat, C., and Parigi, G. (2001) *Solution NMR of Paramagnetic Molecules: Applications to Metallobiomolecules and Models*, Elsevier, Amsterdam, The Netherlands
47. Cunha, C. A., Romao, M. J., Sadeghi, S. J., Valetti, F., Gilardi, G., and Soares, C. M. (1999) *J. Biol. Inorg. Chem.* **4,** 360–374
48. Morelli, X., Czjzek, M., Hatchikian, C. E., Bornet, O., Fontecilla-Camps, J. C., Palma, N. P., Moura, J. J. G., and Guerlesquin, F. (2000) *J. Biol. Chem.* **275,** 23204–23210
49. Siddarth, P., and Marcus, R. A. (1992) *J. Phys. Chem.* **97,** 2400–2406
50. Drosou, V., Malatesta, F., and Ludwig, B. (2002) *Eur. J. Biochem.* **269,** 2980–2988
51. Drosou, V., Reincke, B., Schneider, M., and Ludwig, B. (2002) *Biochemistry* **41,** 10629–10634
52. Page, C. C., Moser, C. C., and Dutton, P. L. (2003) *Curr. Opin. Chem. Biol.* **7,** 551–556
53. Gray, H. B., and Winkler, J. R. (2005) *Proc. Natl. Acad. Sci. U. S. A.* **102,** 3534–3539
54. Nicholls, A., Sharp, K. A., and Honig, B. (1991) *Proteins* **11,** 281–296